Highly efficient and durable III-V semiconductor-catalyst photocathodes via a transparent protection layer

Received 00th January 20xx,
Accepted 00th January 20xx

DOI: 10.1039/x0xx00000x

Shinjae Hwang, [a] James L. Young, [b] Rachel Mow, [b] Anders B. Laursen, [a,d] Mengjun Li,[a] Hongbin Yang,[a] Philip E. Batson,[c] Martha Greenblatt,[a] Myles A. Steiner,[b] Daniel Friedman,[b] Todd G. Deutsch,[b] Eric Garfunkel, [a,*] and G. Charles Dismukes [a,d,*]

Durable performance and high efficiency in solar-driven water splitting are great challenges not yet co-achieved in photoelectrochemical (PEC) cells. Although photovoltaic cells made from III-V semiconductors can achieve high optical-electrical conversion efficiency, their functional integration with electrocatalysts and operational lifetime remain great challenges. Herein, an ultra-thin TiN layer was used as a diffusion barrier on a buried junction n^+p-$GaInP_2$ photocathode, to enable elevated temperatures for subsequent catalyst growth of Ni_5P_4 as nano-islands without damaging the $GaInP_2$ junction. The resulting PEC half-cell showed negligible absorption loss, with saturated photocurrent density and H_2 evolution equivalent to the benchmark photocathode decorated with PtRu catalysts. High corrosion-resistant Ni_5P_4/TiN layers showed undiminished photocathode operation over 120 h, exceeding previous benchmarks. Etching to remove electrodeposited copper, an introduced contaminant, restored full performance, demonstrating operational ruggedness. The TiN layer expands the synthesis conditions and protects against corrosion for stable operation of III-V PEC devices, while the Ni_5P_4 catalyst replaces costly and scarce noble metal catalysts.

Solar energy is, by far, the largest underutilized source of CO_2-free energy.[1] If collected without loss, it could supply the global yearly energy consumed by humans in less than 2 hours.[2] If adequate energy storage were availble,[3] this resource could accelerate future renewable energy usage.[4-6] The solar-driven water splitting process captures solar energy and converts water to its constituent elements of hydrogen and oxygen, which can be efficiently utilized by advanced fuel cell technology.[7]

$GaInP_2$ is the important III-V material for photovoltaic cells, possesses excellent electronic properties and an ideal bandgap (1.8 eV) for potential use as the top (exposed) junction in a tandem PEC device.[8,9] However, $GaInP_2$ is highly unstable in common electrolytes, corroding in acids and alkalis by dissolution or forming oxides (e.g., Ga_2O_3, In_2O_3) that are unstable in applied bias.[10-13] Because the interface has not been successfully passivated yet, its use as PEC photocathode has been limited.[10-12] This instability contrasts with commonly used Si photoabsorbers that are less reactive in acid electrolyte and form a stable oxide.[13] Numerous attempts have been made to protect $GaInP_2$ in PEC devices under hydrogen evolution reaction (HER) conditions.[10,11,14] For example, a thin film of MoS_2 was coated onto p-$GaInP_2$ as a catalyst and protection layer, using a strategy similar to that developed for protection of Si photocathodes.[15,16] This protection layer stabilizes the photocathode for 70 h, but starts to show decrease of activity.[10] Additionally, significant parasitic absorption by MoS_2 and unconverted Mo (~40%) reduces the maximum photocurrent density of the $GaInP_2$ by 30%. Using a so-called graded approach (MoS_2/MoO_zS_y/MoO_x) with transparent TiO_2 layer, the optical losses can be reduced.[11] The resulting g-MoS_2/TiO_2/p-$GaInP_2$ junction achieves saturated photocurrent on par with the unmodified benchmark (bare $GaInP_2$ plus PtRu), which indicates that this approach is successful for improving transparency. However, the device maintained the initial photocurrent density for 20 h but was not tested further hence leaving the corrosion stability unanswered.[11] This method is limited in scope by the choice of materials and inter-diffusional mixing at the catalyst/protection/photoabsorber interfaces during fabrication especially at elevated temperatures. Hence, it precludes the use of buried junctions with n^+-$GaInP_2$ layers (10-20 nm), which are responsible for increasing the photovoltage by as much as 550 mV.[17] Therefore, new, better catalyst-protection layers are required, which do not compromise the

[a] *Department of Chemistry and Chemical Biology, Rutgers University, Piscataway, New Jersey 08854, USA E-mail: egarf@chem.rutgers.edu; dismukes@chem.rutgers.edu*
[b] *National Renewable Energy Laboratory, 15013 Denver West Parkway, Golden, Colorado 80401, USA.*
[c] *Department of Materials Science & Engineering, Rutgers University, Piscataway, New Jersey 08854, USA*
[d] *Waksman Institute, Department of Microbiology, Rutgers University, Piscataway, New Jersey 08854, USA*
Electronic Supplementary Information (ESI) available: See DOI: 10.1039/x0xx00000x

Pursuant to the DOE Public Access Plan, this document represents the authors' peer-reviewed, accepted manuscript. The published version of the article is available from the relevant publisher.

$GaInP_2$ interface, while protecting under the harsh water-splitting conditions.

TiN has excellent physical and chemical properties, including high conductivity and density, hardness, and corrosion resistance.[18] TiN is superior to both TiO_x/Ti and TiO_2 as a diffusion barrier,[19,20] and forms durable interfaces between the photoabsorber and platinum-group-metal-free (PGM-free) HER catalysts (*e.g.*, transition metal phosphides).[21,] It forms a hard protection layer for Si-photocathodes under high-temperature synthesis conditions which enables undiminished stability in PEC operation over 125 h.[21]

Herein, we demonstrate a dual approach to stabilizing the buried junction n^+p-$GaInP_2$ photoabsorber against corrosion without compromising its relevant optical performance, by creating a TiN interface that supports polycrystalline Ni_5P_4, one of the leading PGM-free HER catalysts.[22-24] Superior stability is achieved by combining: 1) low temperature (130 °C) pulsed laser deposition of an ultra-thin TiN film on n^+p-$GaInP_2$ (TiN/n^+p-$GaInP_2$) to preserve thermally unstable $GaInP_2$, and 2) semi-transparent catalyst film of polycrystalline Ni_5P_4 nano-islands (Ni_5P_4/TiN/n^+p-$GaInP_2$). This dual approach achieves photoactivity for HER that is comparable to the benchmark photocathode: PtRu nanoparticles on n^+p-$GaInP_2$ (PtRu/n^+p-$GaInP_2$). Compared to this benchmark, the semi-transparent nano-island Ni_5P_4/TiN/n^+p-$GaInP_2$ photocathode exhibits a slightly improved onset photocurrent ($\Delta\eta$~+120 mV, at -1 mA/cm^2) with decreased fill factor, but an identical saturation photocurrent density using only earth-abundant materials.

Future commercial PEC devices will need to deal with contamination from various metal impurities in the electrolyte that deposit on the electrodes. We developed an effective cleaning treatment to remove surface contamination from electro-deposited Cu ions on the photocathode, introduced by exposure of the copper electrical leads to the electrolyte through crack in the epoxy. A simple acid wash (2M HCl) was developed to selectively etch Cu from the surface and expose the underlying Ni_5P_4, which restores the photocurrent density to its original level. Despite repeating the reactivation procedure twice, the device maintained undiminished performance for 120 h without failure or net loss in photocurrent, limited only by the duration of the test. The high activity and operational stability even after using acid washes to remove common contaminants, is consistent with our previous results on NiP_2/TiN/Si photocathodes,[21] indicating that this protection approach may be generally applicable to other PEC devices.

We fabricated a buried junction n^+p-$GaInP_2$ on a GaAs (100) miscut 4° toward <111>B substrate wafer by epitaxial growth in a custom-built, atmospheric pressure metal organic vapor phase epitaxy (MOVPE) reactor.[25,26] Before performing the surface modification, we studied the effect of various etching solutions (acid, alkaline) for removing the surface oxides on $GaInP_2$ to form a clean and stable interface layer. X-ray photoelectron spectroscopy (XPS) was performed on the bare and etched surface (Figure S1). Peak fitting and reference standards confirm that the bare $GaInP_2$ has surface oxides (when exposed to ambient conditions), identified as Ga_2O_3, In_2O_3, and PO_x which introduce an interfacial layer with low conductivity. Several etching solutions effectively removed the Ga_2O_3 and PO_x signals, but varying residual amount of In_2O_3 was observed for all etchants. Among the tested etching solutions, the *buffered* NH_4F/HF oxide etchant was the most efficient at removing all three of the surface oxides, while not dissolving the $GaInP_2$ substrate.[27] Hence, it was used for the final cleaning.

Figure 1(a) and (b) shows helium ion microscope (HIM) images of the TiN/n^+p-$GaInP_2$ and Ni_5P_4/TiN/n^+p-$GaInP_2$ surfaces.[28] The clean and featureless image in Figure 1(a) demonstrates that the TiN protection layer conformally coats the n^+p-$GaInP_2$ photoabsorber. On the other hand, Figure 1(b) shows that the Ni_5P_4 layer consists of uniform-size crystallites, approximately 20-30 nm in diameter, that are irregularly spaced. These "nano-islands" have similar size and morphology as cubic-NiP_2 on Si(100), as we previously reported. [21] The non-conformal coating of Ni_5P_4 was produced by design, as it serves to minimize undesired parasitic absorption that occurs with conformal coatings of this conducting material.

Optical measurements were performed on Ni_5P_4/TiN deposited on quartz (q-SiO_2) as well as n^+p-$GaInP_2$ substrates to confirm the spectral losses. Figure 1(c) shows the transmittance (T%), reflectance (R%), and absorptance (A%) of the Ni_5P_4/TiN/q-SiO_2. We assumed scattering (S%) is negligible for a polished quartz substrate.[17] The measured absorptance from the Ni_5P_4/TiN layers is 10–15% in the range of 350–700nm wavelengths which is the relevant range for $GaInP_2$.[11] However, a comparison of the total reflectance for bare $GaInP_2$ to Ni_5P_4/TiN/n^+p-$GaInP_2$ (Figure 1(d)) shows a 10-15% decrease by adding Ni_5P_4/TiN on $GaInP_2$. Our previous study of a TiN layer's contribution to reflectance in air and water have shown that the contribution from changing the surrounding media from air to glass and water served as a linear displacement of the total reflection to lower values. This is expected since the glass and water reduce the refractive index change between air and the photoabsorber (we note the similarities in n for Si = 3.9 and $GaInP_2$ = 3.5 at 600 nm)[21,29,30] The results reveal that the light loss caused by absorption in the catalyst and protection layers is compensated by a decrease in reflectance. This indicates that the catalyst-protection layer acts as a partial anti-reflective coating.

The chemical states of the catalyst and interfacial layer were evaluated by X-ray photoelectron spectroscopy (XPS). Figure 2 shows the XPS core level spectra of Ni2p, P2p, Ga2p, and In3d. Both the Ni2p and P2p core levels show the presence of partially oxidized elements. Spectral fitting best describes these as partially oxidized Ni (NiO_x, $2p_{3/2}$: 854.8eV) and phosphorus-oxide (PO_x, $2p_{3/2}$: 132.3 eV), resulting from air-exposure during catalyst synthesis, as previously reported for these catalysts[21,23,31] In addition, a majority component of partially oxidized $Ni^{+\delta}$ ($2p_{3/2}$: 853.8 eV) and reduced $P^{-\delta}$ ($2p_{3/2}$: 129.3 eV) is ascribed to Ni_5P_4, in agreement with previous assignments. [21,23,31] Core level spectra in the Ga2p and In3d region show no Ga or In signals, as expected based on the known mean free path of photoelectrons.[32,33] This confirms that the ultra-thin TiN layer is both conformal and sufficiently robust to prevent atomic diffusion during catalyst formation.

Pursuant to the DOE Public Access Plan, this document represents the authors' peer-reviewed, accepted manuscript.
The published version of the article is available from the relevant publisher.

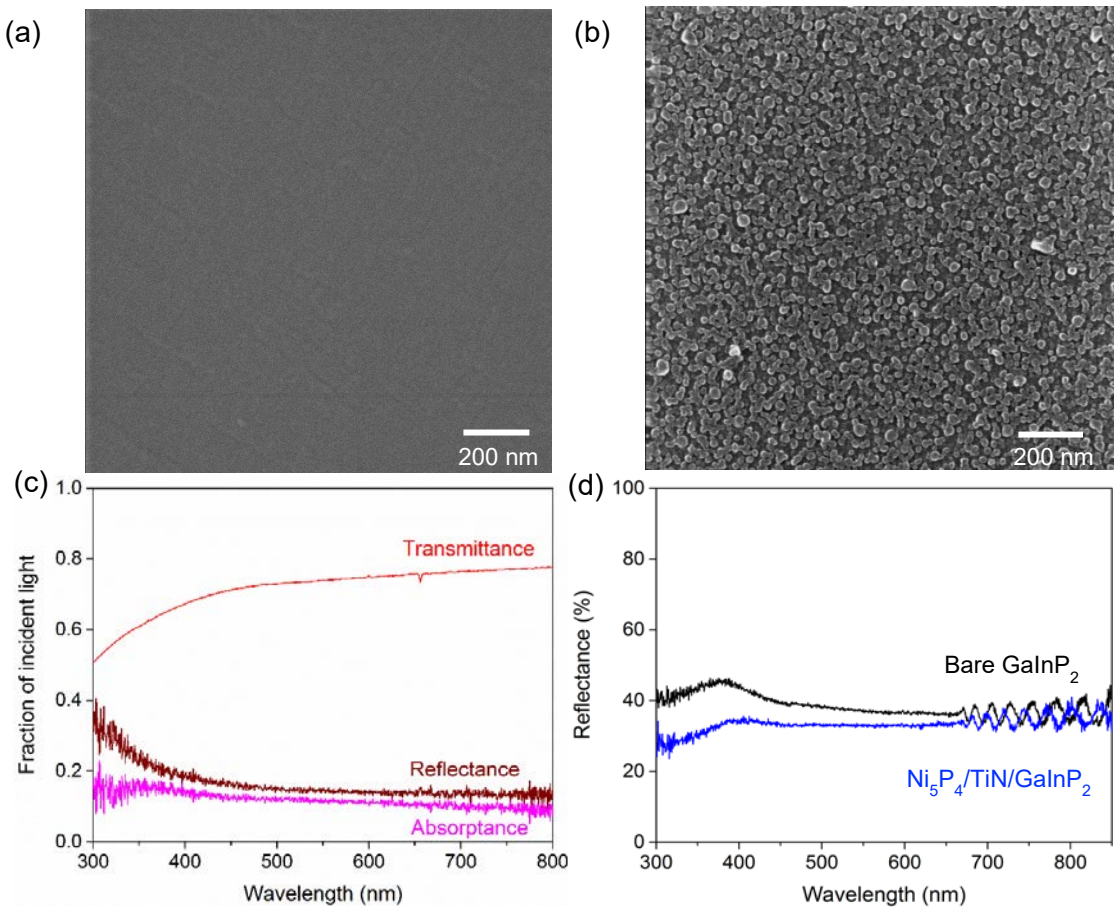

Figure 1 Surface morphologies and optical measurements. Helium ion microscope (HIM) image of (a) TiN modified $GaInP_2$ and (b) Ni_5P_4 on TiN/$GaInP_2$. (c) Optical transmittance (red), reflectance (wine) and absorptance (magenta) of Ni_5P_4/TiN layer on quartz substrate. (d) Reflectance of unmodified bare $GaInP_2$ and Ni_5P_4/TiN modified $GaInP_2$.

Cross-sectional images taken by scanning transmission electron microscope using high angle annular dark field (STEM-HAADF) and energy dispersive spectroscopy (EDS) maps (Figure 3) of the top 80 nm of the device shows the elemental distribution and architecture of the interface. The strong localization of catalyst, protection layer and photoabsorber layers is demonstrated and in agreement with the HIM images. The formation of crystalline Ni_5P_4 nano-islands was verified by lattice fringe distances of 0.340 and 0.274 (±0.02) nm (Figure S2), matching the (110) and (004) d-spacing of Ni_5P_4 respectively. This is further confirmed by X-ray diffraction analysis of a thick Ni_5P_4 film on Si(100) (using the same synthesis) clearly showing polycrystalline Ni_5P_4 (Figure S3). The HAADF image also reveals a 3-4 nm layer under the catalyst of lower contrast. STEM EDS of Ti and N elemental maps identifies this as the TiN protection layer. The absence of both Ga and In (Figure 3) in this layer confirms the diffusion barrier properties of TiN during catalyst synthesis. The O-map shows a significant intensity in the TiN region, indicating that the TiN layer contains a significant amount of oxygen. The relatively low temperature (120°C) and imperfect vacuum level ($1x10^{-3}$ Pa) during the deposition may be the origin of the relatively high oxygen content in TiN.[34] The presence of an oxide shell covering the Ni_5P_4 catalyst, confirms the XPS assignment of surface nickel (NiO_x) and phosphorus (PO_x) oxides. Ni and P EDS maps confirm the 20–30 nm particle diameter.

Photoelectrochemical activity was evaluated in a three-electrode configuration in 0.5M H_2SO_4 electrolyte with 1mM Triton X-100 surfactant (to facilitate bubble detachment) using simulated 1.5 AM G solar illumination (calibrated with an NREL-certified 1.81 eV bandgap $GaInP_2$ reference cell). The catalytic activity of the PtRu/n^+p-$GaInP_2$ benchmark was tested starting with a non-uniform coating of PtRu alloy nanoparticles (2-5nm diameter)[11]. This PtRu alloy nanoparticle catalyst is known to outperform both Pt or Ru alone[20] and shows negligible current loss by parasitic absorption.[11] Figure 4 (a) shows the linear sweep voltammograms (LSVs) of both Ni_5P_4/TiN/n^+p-$GaInP_2$ and PtRu/n^+p-$GaInP_2$. Linear scan voltammograms show the photocurrent onset reaches -1 mA/cm^2 at 1.04 V for Ni_5P_4/TiN/$GaInP_2$ and 0.92 V for the PtRu/$GaInP_2$ benchmark. The positive shift of the photocurrent onset observed for Ni_5P_4/TiN/$GaInP_2$ is likely due to the low intrinsic overpotential of Ni_5P_4 and high loading compared to Pt that we previously reported.[22] The slightly poorer fill factor compared to the PtRu benchmark is probably due to ohmic losses caused by the comparatively higher resistivity in both Ni_5P_4 (630 μΩ · cm) and TiN (30-100 μΩ · cm) compared to Pt and Ru (9.8 and 7.1 μΩ · cm), respectively.[11,21,22,35,36] We note that the actual conductivity of the TiN layer synthesized here, at low

Pursuant to the DOE Public Access Plan, this document represents the authors' peer-reviewed, accepted manuscript.
The published version of the article is available from the relevant publisher.

temperature, would likely be higher due to lattice defects, such as O-insertion.[36] An identical saturated photocurrent density (J_{sat} ~ 8.3 mA/cm^2) reveals that the nano-island morphology of the Ni_5P_4 catalyst and ultra-thin TiN are highly transparent and thus do not compromise the limiting photocurrent density. Also, Figure S4 shows that the Faradaic efficiency for H_2 production for Ni_5P_4/TiN-n$^+$p-GaInP$_2$ at saturated current density is 100%, in agreement with electrocatalysis on pure Ni_5P_4.[22]

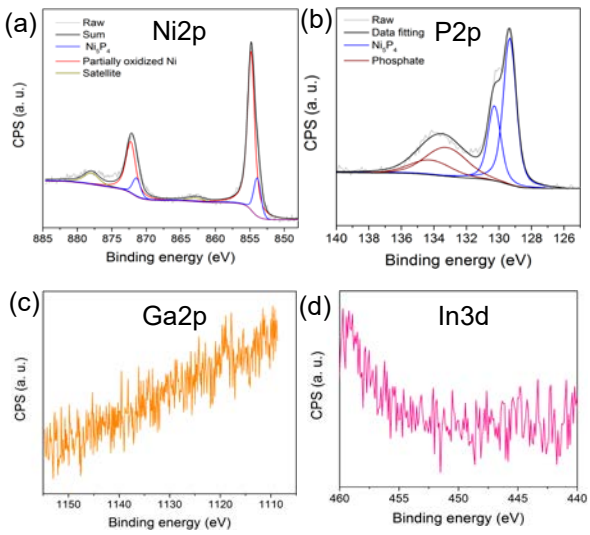

Figure 2 X-ray photoelectron spectra of Ni_5P_4/TiN/GaInP$_2$. (a) Ni2p core level. Peaks were deconvoluted to Ni2p$_{3/2}$, and Ni2p$_{1/2}$ for both Ni_5P_4 (blue), and partially oxidized Ni (red). (b) P2p core level. Peaks were deconvoluted to P2p$_{3/2}$, and P2p$_{1/2}$ for both Ni_5P_4(blue), and phosphate (wine). (c) Ga2p core level (d) In3d core level.

Incident photon to current efficiency (IPCE) was measured using the underfill illumination method, allowing the results to be free from any uncertainty in the measured surface area.[17] The IPCE measurements (Figure 4(b)) confirms the nearly identical spectrally resolved photon-conversion efficiency of the nano-island Ni_5P_4/TiN-n$^+$p-GaInP$_2$ and PtRu/n$^+$p-GaInP$_2$, in the range of 375-700nm. Ni_5P_4/TiN/n$^+$p-GaInP$_2$ show a small increase in IPCE from 300-375nm, which may be attributed to the reduced reflection in this range (Figure 1). The IPCE was integrated over a reference solar irradiance standard (AM 1.5G, ASTM G173-3), and used to determine an accurate saturated current density (J^{IPCE}) of ~ 10.2 mA/cm^2 for both photocathodes. The photocurrent density measured by IPCE is higher than that observed by the LSV measurements, which is attributed to slight discrepancies in the active device-area when masked by epoxy for the LSV measurements. This values is slightly lower than the state-of-the-art GaInP$_2$ PV cell due to the lack of window layer and back reflector.[37]

Photoelectrochemical stability of the devices was evaluated using chronoamperometry (CA) at + 0.25V vs RHE in 0.5M H_2SO_4 using copper leads as contact on working electrode. This potential was selected close to the onset of J_{sat} to allow easy monitoring of small changes to device performance during the test and to avoid exaggeration of device stability. Figure 4(c) shows the CA of Ni_5P_4/TiN/n$^+$p-GaInP$_2$ photocathode, which indicates a slow decrease in photocurrent over the first 24h. Post-reaction XPS after this time shows accumulation of metallic Cu plating (Figure S5). The source of the Cu-contamination was identified as dissolution of the Cu wire and plating on the cathode. The Cu could be selectively removed by immersing in 2M HCl for 3s. XPS analysis (Figure S6) shows the effective removal of Cu and re-exposure of Ni_5P_4. LSVs of Cu contaminated sample (Figure S7) also confirms that Cu contamination shifts the photocurrent onset potential to less positive values (0.83 V vs. RHE) and lower photocurrent density at 0.25 V vs. RHE by covering the active Ni_5P_4 catalyst. However, when the Cu is selectively etched with 2M HCl, the catalytic activity is fully recovered in agreement with the re-exposure of Ni_5P_4 catalyst. The CA experiment was continued in the same configuration and the original photocurrent was restored, followed again by slow deterioration in photocurrent over the next 80 h (104 h total). The surface was again examined by XPS and found to be contaminated with Cu (data not shown). The

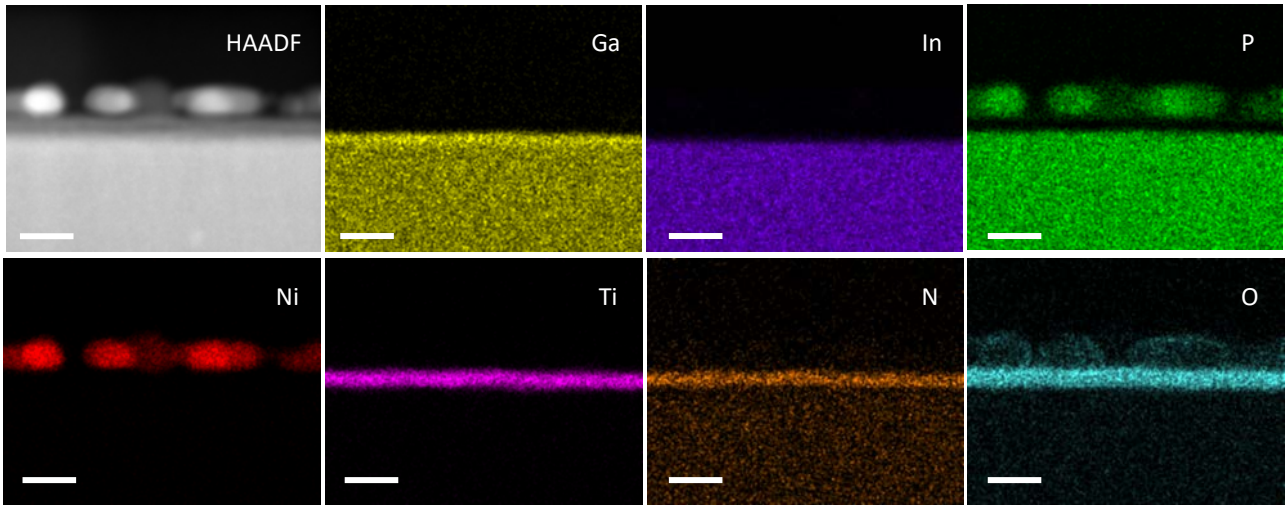

Figure 3 Cross-sectional STEM high angle annular dark field (HAADF) image of Ni_5P_4/TiN/GaInP$_2$ and EDS elemental maps of Ga (yellow), In (purple), P (green), Ni (red), Ti (magenta), N (orange), and O (cyan). Scale bars are 20 nm.

Pursuant to the DOE Public Access Plan, this document represents the authors' peer-reviewed, accepted manuscript. The published version of the article is available from the relevant publisher.

HCl etching was repeated again, and the original operating current was restored. After removal of the Cu contaminant, with undiminished performance. Etching, to remove copper surface contamination on the operating photocathode, restores

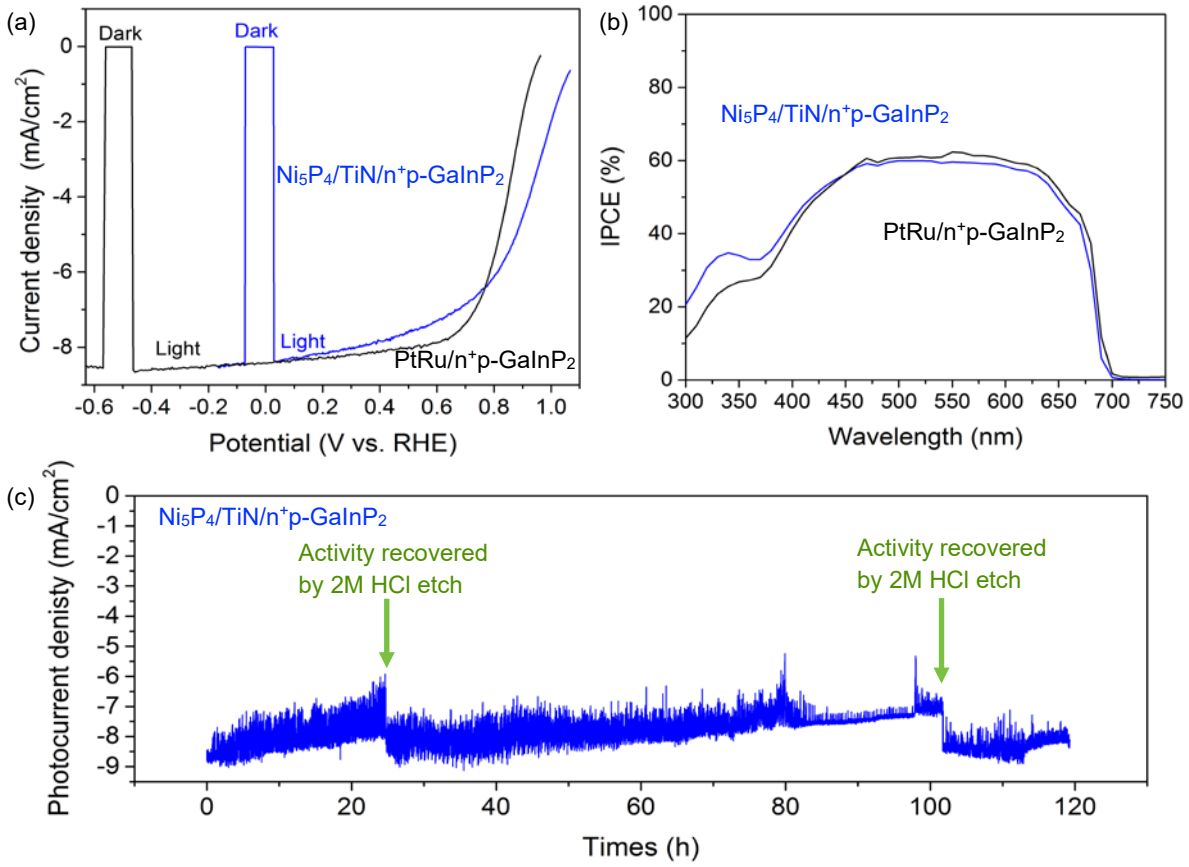

Figure 4 (a) LSVs of Ni_5P_4/TiN/n^+p-$GaInP_2$, and PtRu/n^+p-$GaInP_2$ under light and dark conditions. Scan rate was 20 mV/s (b) IPCE of Ni_5P_4/TiN/n^+p-$GaInP_2$, and PtRu/n^+p-$GaInP_2$. (c) CA of Ni_5P_4/TiN/n^+p-$GaInP_2$ at 0.25 V vs. RHE. Time course shows intentional drift caused by electro-plating of Cu onto photocathode and its removal by etching at 24h and 104h.

stable device performance was recorded for an additional 20 h with no evidence of current loss before termination of the CA run at 120 h (Fig. 4(c)). By contrast, CA analysis of PtRu/n^+p-$GaInP_2$ (Figure S8) shows the photocurrent decreases within 3h, even in the presence of a more cathodically protective applied potential (-0.78 V vs. RHE). This decrease is primarily due to photo-corrosion/dissolution of $GaInP_2$ in the acidic electrolyte.[38] In conclusion, the nano-island Ni_5P_4-TiN catalyst-protection layer performs on par with the PGM-nanoparticle catalyst without protection layer, with respect to catalytic activity and limiting photocurrent density, while exhibiting greatly superior stability against corrosion in electrolyte and even tolerance to mild etching to remove Cu contamination.

In summary, we describe the fabrication and performance of a PGM-free photocathode consisting of semi-transparent nano-islands of Ni_5P_4 catalyst, synthesized on a TiN protection layer on top of n^+p-$GaInP_2$. STEM/EDS and XPS analysis reveal a conformal, ultra-thin, TiN coating that effectively hinders interatomic-diffusion during the high temperature catalyst synthesis. Faradaic efficiency and saturated photocurrent density identical to that of state-of-the-art PtRu/n^+p-$GaInP_2$ benchmark is achieved. The resulting photocathode has negligible optical losses. We show that the catalyst-protection layer provides superior operational stability for at least 120 h the original photocurrent and HER activity, demonstrating the potential for ruggedness and extended lifetime essential for commercial applications.

Conflicts of interest

There are no conflicts to declare.

Author Contributions

S. H. fabricated the Ni_5P_4 catalyst and TiN thin-film and conducted the XPS, XRD, optical measurements, photoelectrochemical measurements, and Faradaic efficiency test. J. L. Y. and R. M. prepared PtRu benchmark catalyst and conducted LSV and IPCE tests. M. L. performed HIM imaging. H. Y. and P. E. B. conducted cross-sectional STEM studies. M. A. S. fabricated the buried junction n^+p-$GaInP_2$. S. H., A. B. L., D. F., T. G. D., M. G., E. G., and G. C. D. designed the experiments. All authors contributed to writing the manuscript.

Acknowledgments

Pursuant to the DOE Public Access Plan, this document represents the authors' peer-reviewed, accepted manuscript. The published version of the article is available from the relevant publisher.

This work was supported by the U.S. Department of Energy, Office of Energy Efficiency and Renewable Energy, Fuel Cell Technologies Office Award#DE-EE0008083. This work was authored in part by the National Renewable Energy Laboratory, operated by Alliance for Sustainable Energy, LLC, for the U.S. Department of Energy (DOE) under Contract No. DE-AC36-08GO28308. Funding provided by U.S. Department of Energy, Office of Energy Efficiency and Renewable Energy, Fuel Cell Technologies Office. The views expressed in the article do not necessarily represent the views of the DOE or the U.S. Government. The U.S. Government retains and the publisher, by accepting the article for publication, acknowledges that the U.S. Government retains a nonexclusive, paid-up, irrevocable, worldwide license to publish or reproduce the published form of this work, or allow others to do so, for U.S. Government purposes. Authors thank to Thermo Fisher Scientific for TEM sample preparation and STEM/EDS mapping.

References

1 G. P. Peters, R. M. Andrew, T. Boden, J. G. Canadell, P. Ciais, C. Le Quéré, G. Marland, M. R. Raupach and C. Wilson, *Nature Climate Change 2012 3:1*, 2012, **3**, 4.

2 N. S. Lewis and D. G. Nocera, *PNAS*, 2006, **103**, 15729–15735.

3 X. Wang, A. Palazoglu and N. H. El-Farra, *Applied Energy*, 2015, **143**, 324–335.

4 J. Turner, G. Sverdrup, M. K. Mann, P. C. Maness, B. Kroposki, M. Ghirardi, R. J. Evans and D. Blake, *Int. J. Energy Res.*, 2008, **32**, 379–407.

5 R. M. Navarro, M. C. Sánchez-Sánchez, M. C. Alvarez-Galvan, F. del Valle and J. L. G. Fierro, *Energy Environ. Sci.*, 2009, **2**, 35–54.

6 Y. Goto, T. Hisatomi, Q. Wang, T. Higashi, K. Ishikiriyama, T. Maeda, Y. Sakata, S. Okunaka, H. Tokudome, M. Katayama, S. Akiyama, H. Nishiyama, Y. Inoue, T. Takewaki, T. Setoyama, T. Minegishi, T. Takata, T. Yamada and K. Domen, *Joule*, 2018, **2**, 509–520.

7 M. Z. Jacobson, W. G. Colella and D. M. Golden, *Science*, 2005, **308**, 1901–1905.

8 S. S. Kocha, D. Montgomery, M. W. Peterson and J. A. Turner, *Sol. Energy Mater. Sol. Cells*, 1998, **52**, 389–397.

9 M. S. Prévot and K. Sivula, *J. Phys. Chem. C*, 2013, **117**, 17879–17893.

10 R. J. Britto, J. D. Benck, J. L. Young, C. Hahn, T. G. Deutsch and T. F. Jaramillo, *J. Phys. Chem. Lett.*, 2016, **7**, 2044–2049.

11 J. Gu, J. A. Aguiar, S. Ferrere, K. X. Steirer, Y. Yan, C. Xiao, J. L. O. Young, M. Al-Jassim, N. R. Neale and J. A. O. Turner, *Nature Energy*, 2017, **2**, 16192.

12 M. Lancaster, R. Mow, J. Liu, Q. Cheek, M. M. MacInnes, M. M. Al-Jassim, T. G. Deutsch, J. L. Young and S. Maldonado, *ACS Appl. Mater. Interfaces*, 2019.

13 M. Pourbaix, *National Association of Corrosion Engineers, Houston*, 1974, 1–648.

14 Y. Wang, J. Schwartz, J. Gim, R. Hovden and Z. Mi, *ACS Energy Letters*, 2019, 1541–1548.

15 A. B. Laursen, T. Pedersen, P. Malacrida, B. Seger, O. Hansen, P. C. K. Vesborg and I. Chorkendorff, *Phys. Chem. Chem. Phys.*, 2013, **15**, 20000–20004.

16 J. D. Benck, S. C. Lee, K. D. Fong, J. Kibsgaard, R. Sinclair and T. F. Jaramillo, *Adv. Energy Mater.*, 2014, **4**.

17 J. L. Young, M. A. Steiner, H. Döscher, R. M. France, J. A. Turner and T. G. Deutsch, *Nature Energy*, 2017, **2**, 17028.

18 N. Biunno, J. Narayan, S. K. Hofmeister, A. R. Srivatsa and R. K. Singh, *Appl. Phys. Lett.*, 1989, **54**, 1519.

19 J. Libardi, K. G. Grigorov, M. Massi, A. S. da Silva Sobrinho, R. S. Pessoa and B. Sismanoglu, *Vacuum*, 2016, **128**, 178–185.

20 J. R. McKone, A. P. Pieterick, H. B. Gray and N. S. Lewis, *J. Am. Chem. Soc.*, 2012, **135**, 223–231.

21 S. Hwang, S. H. Porter, A. B. Laursen, H. Yang, M. Li, V. Manichev, K. U. D. Calvinho, V. Amarasinghe, M. Greenblatt, E. Garfunkel and G. C. Dismukes, *J. Mat. Chem. A*, 2019, **7**, 2400–2411.

22 A. B. Laursen, K. R. Patraju, M. J. Whitaker, M. Retuerto, T. Sarkar, N. Yao, K. V. Ramanujachary, M. Greenblatt and G. C. Dismukes, *Energy Environ. Sci.*, 2015, **8**, 1027–1034.

23 A. B. Laursen, R. B. Wexler, M. J. Whitaker, E. J. Izett, K. U. D. Calvinho, S. Hwang, R. Rucker, H. Wang, J. Li, E. Garfunkel, M. Greenblatt, A. M. Rappe and G. C. Dismukes, *ACS Catal.*, 2018, **8**, 4408–4419.

24 Z. W. Seh, J. Kibsgaard, C. F. Dickens, I. Chorkendorff, J. K. Nørskov and T. F. Jaramillo, *Science*, 2017, **355**, eaad4998.

25 B. A. MacLeod, K. X. Steirer, J. L. Young, U. Koldemir, A. Sellinger, J. A. Turner, T. G. Deutsch and D. C. Olson, *ACS Appl. Mater. Interfaces*, 2015, **7**, 11346–11350.

26 D. J. Friedman, S. R. Kurtz, K. A. Bertness, A. E. Kibbler, C. Kramer, J. M. Olson, D. L. King, B. R. Hansen and J. K. Snyder, *Prog. Photovolt. Res. Appl.*, 1995, **3**, 47–50.

27 C.-T. Lee, H.-P. Shiao, N.-T. Yeh, C.-D. Tsai, Y.-T. Lyu and Y.-K. Tu, *Solid-State Electronics*, 1997, **41**, 1–5.

28 M. T. Postek and A. E. Vladar, *Scanning*, 2008, **30**, 457–462.

29 D. E. Aspnes and A. A. Studna, *Phys. Rev. B*, 1983, **27**, 985–1009.

30 E. Ochoa-Martinez, L. Barrutia, M. Ochoa, E. Barrigon, I. Garcia, I. Rey-Stolle and C. Algora, *Sol. Energy Mater. Sol. Cells*, 2018, **174**, 388–396.

31 J. Kibsgaard, C. Tsai, K. Chan, J. D. Benck, J. K. Nørskov, F. Abild-Pedersen and T. F. Jaramillo, *Energy Environ. Sci.*, 2015, **8**, 3022–3029.

32 S. Tanuma, C. J. Powell and D. R. Penn, *Surf. Interface Anal.*, 1991, **17**, 927–939.

33 M. V. Lebedev, W. Calvet, B. Kaiser and W. Jaegermann, *J. Phys. Chem. C*, 2017, **121**, 8889–8901.

34 R. Chowdhury, R. D. Vispute, K. Jagannadham and J. Narayan, *J. Mater. Res.*, 1996, **11**, 1458–1469.

35 R. W. Powell, R. T. and M. J. Woodman, *Platinum Metals Rev.*, 1962, **4**, 138–143.

36 R. D. Vispute and J. Narayan, *J. Electron. Mater.*, 1992, **25**, 1–4.

37 S. Essig, S. Ward, M. A. Steiner, D. J. Friedman, J. F. Geisz, P. Stradins and D. L. Young, *Energy Procedia*, 2015, **77**, 464–469.

38 O. Khaselev and J. A. Turner, *J. Electrochem. Soc.*, 1998, **145**, 3335–3339.

Pursuant to the DOE Public Access Plan, this document represents the authors' peer-reviewed, accepted manuscript. The published version of the article is available from the relevant publisher.